

# Industrial Design of Axisymmetrical Devices Using a Customized FDTD Solver from RF to Optical Frequency Bands

■ Malgorzata Celuch and Wojciech K. Gwarek

The turn of the century has connotations of impending radical changes. Impending does not mean instantaneous. The 19th century *fin de siècle* spanned nearly four decades of alterations structural for the present industrialized society. Our contemporary *fin* is still in motion but has already reshaped the world. Many of these changes have a touch of microwaves: we communicate via mobile phones and Internet, microwave ovens spread into more and more households, and we use radio frequency identification (RFID) technology in offices and on skiing vacations. However, what microwave professionals are likely to emphasize as a major change, is a nearly paradigmatic shift in how an engineer performs his or her job.

## Microwave Design: Where Analytical and Numerical Approaches Interleave

Four decades ago, microwave engineers were routinely applying well-known design skills and Smith charts. Empirical formulas or numerically generated look-up tables came to help

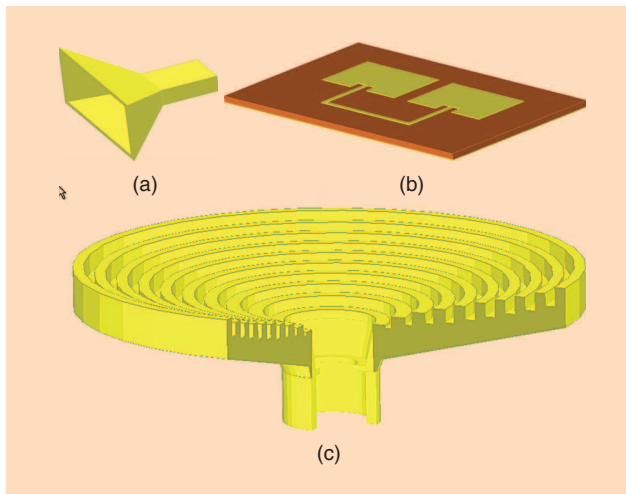


**Figure 1.** Examples of microwave antennas where structure symmetries can be exploited in the modeling or problem dimensionality reduced: (a) pyramidal horn antenna—a full 3-D problem with an option of two symmetry planes, (b) planar Van Atta antenna—a 2.5-D problem solvable by the generic 2.5-D MoM, (c) axisymmetrical corrugated horn antenna—a V2-D problem in cylindrical coordinates.

Malgorzata Celuch ([m.celuch@ire.pw.edu.pl](mailto:m.celuch@ire.pw.edu.pl)) and Wojciech K. Gwarek ([w.gwarek@ire.pw.edu.pl](mailto:w.gwarek@ire.pw.edu.pl)) are with the Institute of Radioelectronics, Warsaw University of Technology, ul. Nowowiejska 15/19, 00-665 Warsaw, Poland.

Digital Object Identifier 10.1109/MMM.2008.929686

where analytical solutions of the Maxwell equations could not be obtained. Early microwave computer-aided design (CAD) was essentially a digitized and automated form of the above techniques and databases. Electromagnetic (EM) software was gradually being developed but was considered a luxury or a fancy. It could hardly be applied to anything like a practical task outside leading laboratories equipped with expensive mainframe computers.

Today, microwave design and EM software are closely linked and running on PCs and laptops. Fully three-dimensional (3-D) numerical solvers have proliferated from academia via research institutes into a majority of industrial enterprises. It is not unusual for a lab to have at least two different tools for cross-comparison purposes, for example, one based on the finite difference time method (FDTD) [1]–[4] and the other on the more classical finite element method (FEM) [5], [6] in the frequency domain. The engineer's vision is no longer constrained by the necessity to manufacture and physically measure a specimen of a new device. Software prototyping reduces the design costs and opens way to new technologies previously beyond imagination. Numerical 3-D models of microwave antennas [such as the pyramidal horn antenna of Figure 1(a)], transmission line components, resonators, and the like are effectively evaluated in a virtual laboratory.

However, with so many limitations removed, the engineer's desire for experimenting with more sophisticated concepts or complete large-scale designs ever increases. Computational EMs may never reach the era of all such problems being solved by brute force by the general purpose software. Therefore, there remains a need for customized modeling methods, each invented for a specific range of microwave applications. This is exemplified by the still unparalleled position of the two-and-a-half dimensional (2.5-D) method of moments (MoM) as the design tool for predominantly planar structures [7], [8] such as the Van Atta patch antenna of Figure 1(b).

However, there is also another trend to be noted, which will be our focus further on. Rather than starting from a generic semi-analytical method (for example, a purely planar MoM), and supplementing it with advanced numerical models (for example, of vias and vertical metal strips) to extend its scope of applications, one may also reverse the way of thinking. What if one starts with a general purpose 3-D numerical solver and improves its efficiency by incorporating some analytical knowledge of field patterns in a particular set of structures?

## Symmetries and Beyond

The FDTD algorithms applied in commercial software are nearly all based on 3-D spatial discretization in Cartesian coordinates. This is the most versatile but not necessarily the most effective way of representing the EM space. In many

cases, full EM information about the device can be extracted from fields in a subregion. Utilization of structure symmetries with respect to principal planes of the coordinate system is best known and typically possible in the commercial software. It allows economizing on the computer resources by, for example, a factor of four in the analysis of pyramidal horn antennas such as the one of Figure 1(a), but never more than a factor of eight in the 3-D space.

One may economize more if one knows more about the structure. In a rectangular waveguide H-plane horn, the geometry and the fields remain invariant in one dimension, which therefore does not need to be discretized. Some 3-D software packages have a dedicated two-dimensional (2-D) analysis option, but even if not, the user may simply set up a one-layer model.

More difficult to exploit is a 2-D nature of structures where the geometry remains invariant in one dimension but the fields do not. In fact, by virtue of the boundary conditions, the fields will then be harmonic, i.e., exhibiting sine or cosine dependence on this spatial coordinate. This class of problems was distinguished as vector two-dimensional (V2-D) [9] and systematically examined by Gwarek et al. [10]. Waveguide discontinuities in the E-plane are one example of a Cartesian V2-D problem, with fields harmonic across the guide width. Another example is the analysis of modes and dispersion characteristics in arbitrary transmission lines, where the field at a particular frequency is harmonic along the guide. The latter case attracted a lot of research effort in the 1990s and led to several algorithms [11]–[17] subsequently compared in [18]. Note that a V2-D solver, in either time- or frequency-domain, is often used as a preprocessor in a general purpose 3-D pack-

age for generating modal field patterns at ports, but the results may not be externally accessible to the user.

The key point is that reducing the 3-D Cartesian geometry to a rigorous 2-D model saves, as a rule of thumb, over an order of magnitude in computer effort.

### Do Engineers Think Cartesian?

Let us challenge the other commercial assumption, namely, using a Cartesian coordinate system as a reference. In FEM, this choice does not constrain the meshing, which is irregular and nonorthogonal. In early FDTD, stair-case meshes resulted and hindered practical applications of the method. While several valuable works have been reported on nonorthogonal and unstructured FDTD grids [1, Ch.11], they have a predominantly research flavor. Commercial FDTD packages enhance basic Cartesian meshing with some forms of locally boundary conforming elements [2]–[4].

We may tend to think in Cartesian coordinates in our everyday life, but these are not the best coordinates for modeling, e.g., a corrugated circular horn antenna as in Figure 1(c). A cylindrical coordinate system would be more appropriate, allowing precise geometry approximation even on a relatively coarse mesh. What we actually advocate as a tool of choice for the axially symmetrical devices is a combination of the two: change of the coordinates and utilizing the V2-D assumption in the cylindrical system.

### V2-D FDTD in Cylindrical Coordinates—Body of Revolution FDTD

Structures maintaining axial symmetry of the boundary conditions belong to the class of V2-D problems in the cylindrical coordinates [10]. The total EM field in such structures can be decomposed into a series of orthogonal modes, with different angular field dependence of the  $\cos(n\varphi)$  or  $\sin(n\varphi)$  type, where  $\varphi$  is angular variable of the cylindrical coordinate system and  $n = 0, 1, 2, \dots$ . As shown in [10] or [1, Ch. 12], each  $n$ -mode is decoupled from the remaining ones and can be analyzed separately. The numerical simulation can be conducted in 2-D, over one half of the long-section of the structure, with  $n$  predefined as a parameter.

Note that for the cylindrical V2-D FDTD, economies of computer effort with respect to the 3-D meshing are typically higher than for the Cartesian V2-D. This is due to the additional gains with accurate representation of cylindrical surfaces, corrugations, and slots. As a rule-of-thumb, over two orders of magnitude savings in RAM and CPU usage is expected.

Publications on V2-D FDTD, also known as body of revolution (BOR) FDTD, are numerous, but each tends to address a specific problem type: wake fields and impedances of particle accelerators [19],

#### Scope of Software Applications

The conformal BOR FDTD method handles a variety of practical problems including [2]:

- calculations of radiation patterns, gain, radiation efficiency, and return loss of axisymmetrical antennas of various types (horn, rod, biconical), rigorously taking into account irregular geometry, complicated corrugations, and inhomogeneous filling
- calculations of radiation patterns and radiation resistance of small dipole or loop radiators, located at the axis of the cylindrical coordinate system
- fast full-wave analysis of coaxial connectors; automatic connector design by running multiple EM analyses in optimization loops
- accurate S-parameter calculations of circular waveguide discontinuities, also in cases involving strong dispersion and multimodal propagation
- determination of eigen frequencies, Q-factors, and pure modal field patterns for shielded and open inhomogeneous axisymmetrical resonators, also in cases involving closely-spaced modes or whispering gallery modes
- calculation of heating patterns and specific absorption rate in axisymmetrical bodies.

The numerical modeling is conducted in the 2-D long-section, with angular field dependence enforced analytically. In comparison with the 3-D discretization by general purpose software, economies in computer effort by over two orders in magnitude are achieved.

[20]; coaxial connectors [21]; optical lenses [22]; transverse electromagnetic wave (TEM) antennas [23], [24]; or cylindrical resonators [25]. Moreover, in most cases, only scalar 2-D problems with  $n = 0$  and three non-zero field components are considered. In [1, Ch.12] and [25], theoretical derivations are provided as a function of  $n$ , but the examples remain of the scalar type. In [10], the theory has been fully implemented for an arbitrary  $n$ , and this is the approach followed by our research group since. We have added new functions for near-to-far field transformation [26], robust modeling of on-axis singularities [27], conformal meshing (see “Conformal Meshing”), dispersive media, wide band modeling of lossy metals, logarithmic and hyperbolic meshing [27], features relevant for microwave heating applications, signal postprocessing methods after [28], and many more.

The theory will not be further summarized as we do not consider it the most relevant issue for the readership of *IEEE Microwave Magazine*, and it is available elsewhere. There is, however, a piece of a good news for engineers who do *think Cartesian* and are reluctant to switch the coordinates. The BOR FDTD model can be conveniently interpreted through an equivalent Cartesian circuit. The model is shown in “Interpretation of Cylindrical BOR FDTD as a Cartesian Planar Circuit.”

We have worked for two decades on the FDTD theory as well as popular FDTD codes. In this article, we will try to highlight several applications, which we consider representative of BOR FDTD and its implementation in the QW-V2D package [2]. The specific constellation of examples reflects our experience in the support of microwave and antenna engineers. The article is, in a way, a collated review of cases where BOR FDTD has been found a breakthrough in the design strategies.

One more remark is appropriate with regard to the computer resources actually used. Throughout the article, we apply discretization corresponding to the final fine-tuning of

the design. It has been verified to suppress the numerical errors below uncertainties of material parameters and mechanical tolerances. This is much finer than meshing typically used at the early stages of concept development or during preliminary optimization. Still, due to the BOR FDTD natural computational effectiveness and the specific features of QW-V2D, the recorded usage of computing times and RAM is modest.

### Example 1: Coaxial Output of a Traveling Wave Tube

Our first example concerns optimization of transmission through a coaxial structure used as an output of a traveling wave tube (TWT). Since TWT is a vacuum device, its output should include a so called vacuum window, i.e., a ceramic barrier separating the vacuum part from the open-air part. Applicable ceramics have high permittivity, and usually, alumina of relative permittivity about ten is applied. The unit capacitance of the coaxial line section including a ceramic ring is therefore much higher than that of the air or vacuum sections. To avoid local mismatch, the line’s unit inductance must be increased. This can be achieved by increasing the diameter of the external conductor or/and introducing a meander type of path for the currents in the line. However, such solutions may introduce a resonant behavior of the structure limiting its operating frequency band.

Figure 2(a) presents a longitudinal section of TWT output integrated with a coaxial N-type connector (shown in the right part of the picture). The coaxial connector includes two teflon rings (marked in gray). The ceramic insert (marked in orange in the left part of the picture) is adjacent to a wide section of the coaxial line with a reentrant cavity to compensate high capacitance introduced by the ceramic. It was originally designed for a TWT working up to 4 GHz and positively verified in practical applications. Then the manufacturer tried to

### Conformal Meshing

Meshing of a simple horn antenna, with shallow opening (yellow—metal, blue—air): conformal mesh generated by QW-V2D (upper) versus classical staircase mesh (lower). Conformal meshing offers further computer run time savings for large problems or intricate geometries, compared with stepped edge modeling. In QW-V2D conformal meshing does not require FDTD time step reduction.

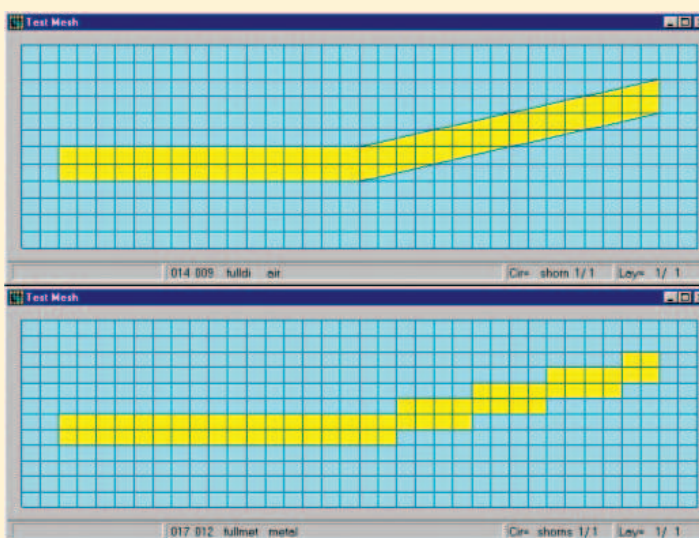


Figure S1. Conformal meshing.

apply a similar solution for a frequency band about 10 GHz— with a negative effect. This can be explained by the results of simulation of the reflection coefficient  $|S_{11}|$  versus frequency, as presented in Figure 3 (red line). The structure exhibits a resonant behavior with full reflection at 13.5 GHz. The field dis-

tribution at 10 GHz (Figure 4) suggests that the origin of that behavior is the re-entrant cavity adjacent to the ceramic ring.

The simulation was performed using QW-V2D software with axisymmetrical excitation by the TEM mode. Thus the problem was reduced to a scalar 2-D one, with only three

### Interpretation of Cylindrical BOR FDTD as a Cartesian Planar Circuit

We consider two structures: One constructed as a body of revolution of contour C and the other as a rectangular prism built by vertical extrusion of the same contour. We use the following transformations of coordinates, media parameters, and field components.

#### a) Original BOR structure

Coordinates:  $x, \rho, \varphi$  with  $0 < \varphi < 360^\circ$

#### b) Equivalent structure in Cartesian coordinates

$x' = x, y' = \rho, z' = \varphi/360$   $0 < z' < 1$

Media parameters:

$$\varepsilon = \begin{bmatrix} \varepsilon & 0 & 0 \\ 0 & \varepsilon & 0 \\ 0 & 0 & \varepsilon \end{bmatrix} \quad \mu = \begin{bmatrix} \mu & 0 & 0 \\ 0 & \mu & 0 \\ 0 & 0 & \mu \end{bmatrix} \quad \varepsilon' = \begin{bmatrix} \varepsilon y' & 0 & 0 \\ 0 & \varepsilon y' & 0 \\ 0 & 0 & \varepsilon / y' \end{bmatrix} \quad \mu' = \begin{bmatrix} \mu y' & 0 & 0 \\ 0 & \mu y' & 0 \\ 0 & 0 & \mu / y' \end{bmatrix}$$

Field variables:

$$E_x, E_\rho, E_\varphi, H_x, H_\rho, H_\varphi,$$

$$E'_x = E_x; E'_y = E_\rho; E'_z = E_\varphi y';$$

$$H'_x = H_x; H'_y = H_\rho; H'_z = H_\varphi y';$$

It can be proven that the field distributions  $E_x, E_\rho, E_\varphi, H_x, H_\rho, H_\varphi$  obtained by solving Maxwell equations in structure (a) are the same as the field distributions  $E'_x, E'_y, E'_z, H'_x, H'_y, H'_z$  obtained by solving Maxwell equations in structure (b).

Additional comments on the used transformations, boundary conditions, and modes propagating in both structures can be made:

- The height of the equivalent structure (b) is equal one in any units we choose. However, the other dimensions must be expressed in the same units. Thus the choice of the unit influences also normalization of the permittivity, permeability and field components making the system consistent regardless if we choose the unit to be 1 m, 1 inch or 1 mm. In any case, the field distribution along the  $z'$ -axis is analytically known and the space in that direction does not need to be meshed during the electromagnetic analysis. The circuit size in that direction is a purely formal notion with no influence on the analysis.
- In the case of BOR structures boundary conditions in the  $\varphi$  direction are periodic. Thus in the equivalent rectangular structure we should only consider modes producing  $n \cdot 360^\circ$  phase shift along  $z'$ -axis. Both types of solutions: those proportional to  $\cos(n \varphi)$  and those proportional to  $\sin(n \varphi)$  are valid and thus in the equivalent circuit (b) we may assume either PEC or PMC conditions at  $z' = 0$  and  $z' = 1$ .
- For the axisymmetric fields ( $n = 0$ ), the propagating modes can be separated into two sets having no influence on each other. One of those sets is composed (in the original circuit) of only  $E_x, E_\rho, H_\varphi$  components. It includes the TEM coaxial mode and all the waveguide modes of  $TM_{0m}$  types (with  $m = 1, 2, \dots$ ). The other set composed of  $E_\varphi, H_x, H_\rho$  components includes all the cylindrical waveguide modes of  $TE_{0m}$  types. Each of the sets of modes is described by a scalar wave equation. Thus we can consider two independent scalar 2-D problems.
- For higher angular field dependence ( $n > 0$ ) all field components can coexist in a mode. For each  $n$  we have one 2-D problem with six field components. One simulation concerns all cylindrical waveguide modes of types  $TM_{nm}$  and  $TE_{nm}$  (with  $n$  fixed and  $m = 1, 2, \dots$ ).

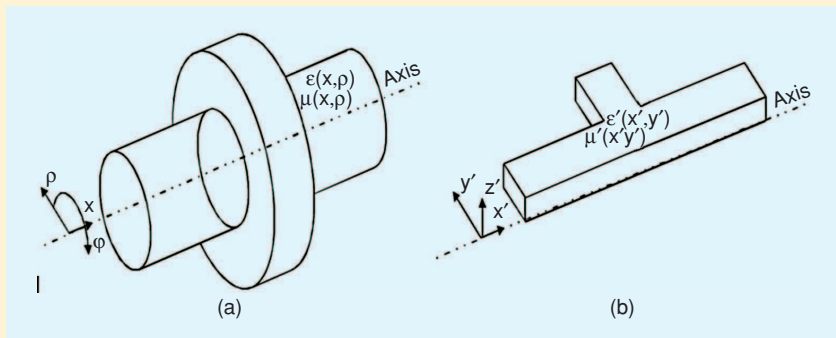
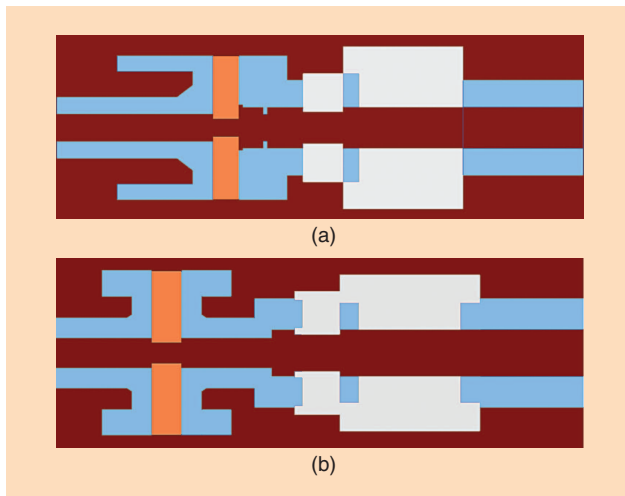
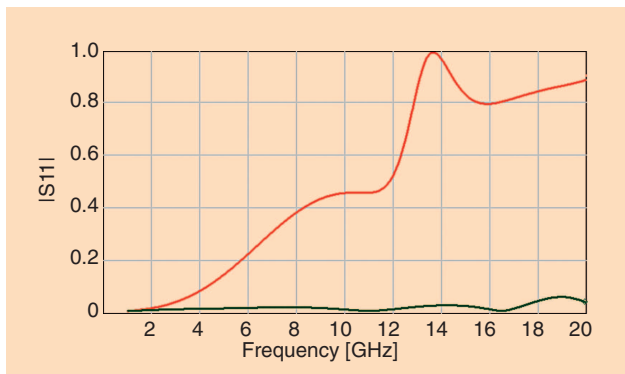


Figure S2. Interpretation of cylindrical BOR FDTD as a Cartesian planar circuit.

non-zero field components ( $E_x, E_\rho, H_\phi$ ). As a consequence, its FDTD analysis is very fast. Even with relatively dense meshing (as shown in Figure 4), the analysis takes only about



**Figure 2.** Long section of a TWT output including a ceramic vacuum barrier (orange): (a) N-type connector in the original form and (b) after optimization. Metal parts are marked in brown, teflon parts in gray and vacuum/air in blue. The length of the structure is 25 mm in (a) and 22 mm in (b). Diameter of the ceramic ring is 10.5 mm in both cases. The output (on the right) is a 7 mm 50  $\Omega$  line.



**Figure 3.** Reflection coefficient  $|S_{11}|$  versus frequency of the structure of Figure 2(a) (red line) and Figure 2(b) (green line).

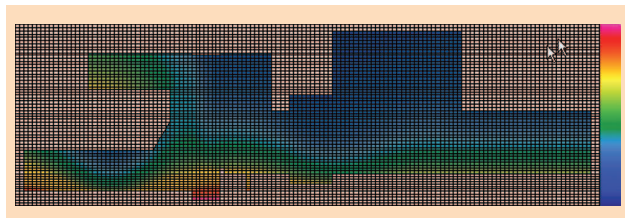


**Figure 4.** Distribution of the time-maximum value of angular  $H$  component across the structure of Figure 2(a) at 10 GHz. Logarithmic scale with a span of 20 dB between the lowest value (blue) and the highest value (purple) is used. Field variation along the coaxial line in the left part of the picture indicates a high reflection coefficient. Concentration of the magnetic field in the upper left part suggests a resonant behavior of the re-entrant cavity. The grid shows the actual FDTD meshing used in simulations.

5 s on a laptop computer with a 2.4 GHz clock. This brings automatic optimization with many variables within reach. Contrary to the general purpose 3-D approach, one calculation of the goal function becomes relatively inexpensive. Moreover, fine discretization limits the level of the numerical noise. Both factors contribute to the successful application of most classical optimization methods.

The result of optimization of the considered structure is presented in Figure 2(b). The structure is not dramatically different from the original one, but it exhibits quite remarkable performance with  $|S_{11}|$  smaller than 0.045 in the entire band of application of N-connectors (up to 18 GHz).

### Example 2: A Millimeter Wave Gaussian Beam Forming Antenna

Example 1 was very effectively calculated using a 2-D FDTD software. However, its solution with a general purpose 3-D FDTD and contemporary PC hardware would also be possible, though quite time consuming. This may not be the case when structures much bigger than the wavelength must be modeled, for example, in optical or millimeter-wave quasi-optical devices as exemplified in Figure 5.

The setup consists of a big radiating horn with 60 corrugations and a teflon lens in front of it. It is supposed to form a Gaussian beam with a waist of about 10 cm in diameter at a distance of about 70 cm from the horn. Quasi-TEM properties of the wave in the waist are needed for investigating material properties at millimeter frequencies [29]. Here, the frequency of 26.5 GHz was considered. Simulation of the Gaussian beam-forming properties requires a cylindrical domain of about 100 cm length and 30 cm diameter. In the general purpose 3-D approach, this entails a simulation domain of about  $88 \times 27$  wavelengths in air. Assuming an average of about 15 FDTD cells per wavelength (due to required denser meshing in the dielectric and in the horn areas), we obtain a requirement of about 216 million of FDTD cells. This necessitates about 20 GB of computer RAM and rather impractical computing time of the order of 20–60 hours, depending on the computer speed.

The requirements reduce dramatically for a customized V2-D FDTD simulation. We need about 0.45 million of cells, 40 MB of memory and the computing time of about 12 minutes.

Figure 5(a) presents a time-maximum value of the E-field in the long section of the structure. The scale is logarithmic with 60 dB span between the maximum value (purple) and the minimum value (blue). We can see that a Gaussian beam waist is formed in the region of the cross-section marked S2. Electric field in the waist is about 20 dB lower than in the feeding guide. The electric field distribution in the cross section S2 presented in Figure 5(d) confirms good symmetry. It is interesting to note that the field is not axisymmetrical in the cross section S1 (in front of the lens) as shown in Figure 5(c). The results presented in Figure 5 have been confirmed by independent experiments presented in [29].

### Example 3: A Large Dual Reflector Antenna

Another area of applications where the size of objects is large compared to the wavelength is parabolic reflector antennas

design. Single-reflector front-fed antennas are traditionally designed by domain decomposition. The feeding horn alone is rigorously modeled and its far fields patterns are extracted. Then asymptotic methods such as physical optics are used to couple the full-wave results with the reflector description. However, this approach is difficult to apply in the case of a Gregorian type two-reflector antenna as in Figure 6. The feeding horn radiates towards the primary reflector, which reflects the radiation towards the main reflector forming the beam. The feeding horn and the primary reflector are close to each other, and the primary reflector shadows part of the radiation from the main reflector. Ideally, the entire structure should be analyzed by the full-wave methods to design the feed in its operational environment. However, the size of the entire structure often exceeds hundred and sometimes reaches several hundreds of wavelengths. This leaves a capability gap where asymptotic methods are not sufficiently accurate but the antenna is too large to be modeled economically in a general purpose 3-D software. On the other hand, the V2-D approach remains computationally effective, as we will show.

Consider an antenna of a dish diameter about 150 cm working in the frequency band around 8 GHz. The antenna diameter is therefore equal to about 40 wavelengths. The required domain of simulations would be about  $50 \times 50 \times 30$  wavelengths in a 3-D software but it reduces to easily manageable  $25 \times 30$  wavelengths in the rigorous V2-D model. Figure 7 presents the calculated input guide reflection coefficient ( $|S_{11}|$ ) versus frequency in the band of 7–9 GHz. The red curve corresponds to the original design. The reflections are relatively low but contain several ripples. The ripples of the large period (about 0.6 GHz) can be associated with the reflections from the primary reflector while the denser ripples—with the reflections from the main reflector.

Figure 8 presents the far-field radiation patterns for the H-plane (red) and E-plane (blue) calculated at 7.8 GHz. The main beam has the directive gain of more than 40 dB and has the 10 dB width of about  $1.3^\circ$ . The radiation patterns reveal one troubling effect. The H-plane pattern exhibits a relatively high radiation around  $90^\circ$ . This is so called spillover, which may be quite harmful for the signal-to-noise ratio of the system.

To investigate the problem, we have calculated time-maxima of the angular electric field component in the H-plane [Figure 9(a)] and angular magnetic field component in the E-plane [Figure 9(b)]. Both field distributions are presented in a logarithmic scale with a span of 60 dB between the highest values (purple) and the lowest values (dark blue). While the distributions are quite similar within the corrugated horn, they differ substantially in the area between the reflectors. The H-plane beam is split into three parts forming a kind of a space resonant mode. We can suspect that the middle part of the beam causes a spurious reflection from the edges of the primary reflector and is responsible for the higher radiation at about  $90^\circ$ . From the field distributions in the upper part of the two pictures, it becomes clear that the spillover of the H-plane pattern is significantly higher.

Figure 9 suggests that the spillover problem may originate at the edge of the primary reflector. Thus we introduce certain

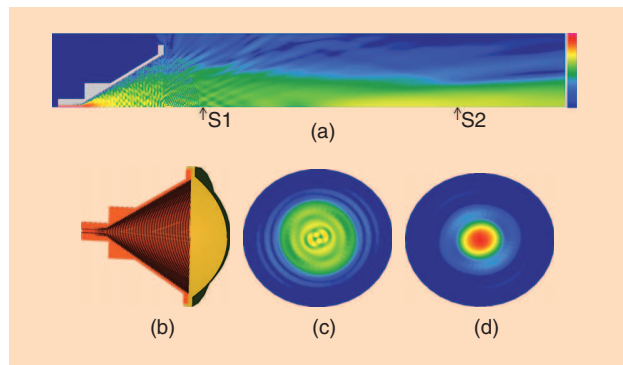


**Figure 5.** A Gaussian beam forming device for material measurements at millimeter wavelengths: (a) time-maximum value of the E-field in the long section of the structure, (b) general view of the horn and the lens, (c) electric field in front of the lens (S1 Section), and (d) electric field in the waist (Section S2).

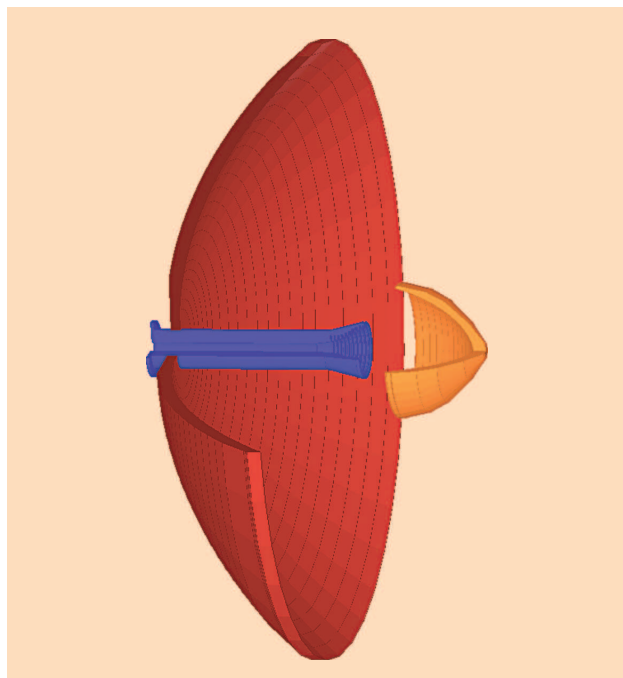


**Figure 6.** A Gregorian type two reflector antenna.

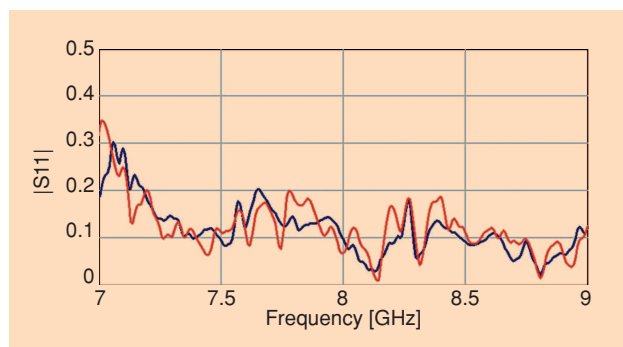


**Figure 7.** Reflection coefficient of the antenna of Figure 6 in its original form (red) and after modification (blue).

modifications. The primary reflector is cut and one corrugation is introduced in it. The results of the analysis with the

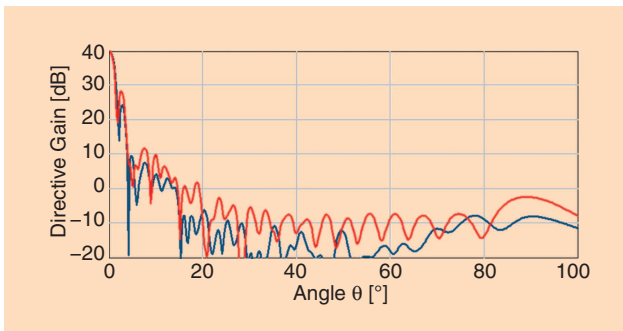


**Figure 8.** E-plane (red) and H-plane (blue) radiation patterns of the antenna of Figure 6.

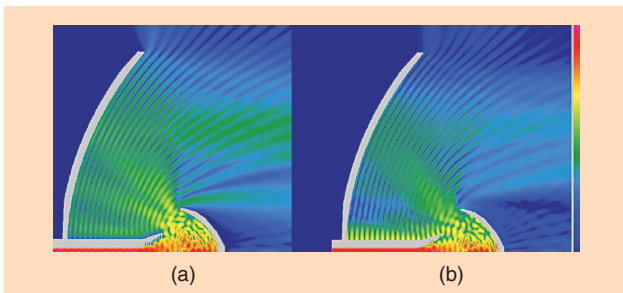


**Figure 9.** Time-maxima of the (a) angular electric field component in the H-plane and (b) angular magnetic field component in the E-plane in the antenna of Figure 6.

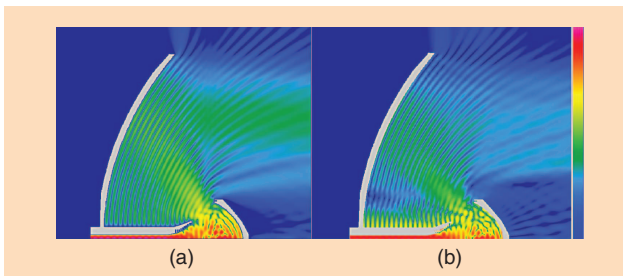


**Figure 10.** (a) Time-maxima of the angular electric field component in the H-plane and (b) angular magnetic field component in the E-plane in the antenna of Figure 6 after modification.

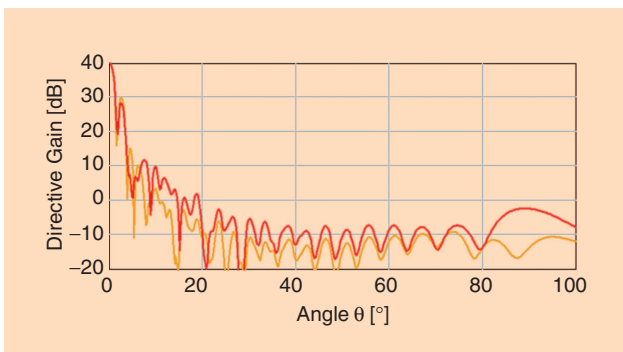


**Figure 11.** H-plane radiation patterns of the antenna of Figure 6 in its original form (red) and after modification (orange).

modified reflector are presented in Figure 10. The field distribution for the H-plane has changed, with respect to the original one of Figure 9. The main beam between the reflectors is more smooth and unsplit. As a result, the H-plane spillover is reduced by almost 10 dB, as confirmed by the radiation patterns of Figure 11. The original pattern is presented in red while the new one in orange. Interestingly, the  $|S_{11}|$  characteristic has also changed. The  $|S_{11}|$  curve presented in blue in Figure 7 is more smooth, indicating reduced reflections from the main reflector reaching back the horn feed.

#### Example 4: A Multimode Dielectric Resonator

Consider a cylindrical dielectric resonator (marked red in Figure 12) coupled to two microstrip lines on a substrate plate (marked green in the lower part of the structure). When applying such resonators in telecommunication filters, we often try to excite so called whispering gallery modes. These are the modes of high angular variation. The field of such modes concentrates close to the circumference of the dielectric cylinder and decays very rapidly outside the dielectric. It becomes negligible close to the metal walls of the box containing the filter. Hence the unloaded Q-factor of the resonator is determined only by the losses of the dielectric material, and may be very high.

However, whispering gallery modes are difficult to analyze. Their resonant frequencies are much higher than that of the dominant mode. Many modes of different angular index  $n$  may resonate at the frequencies very close to one another. This is exemplified by the 3-D FDTD analysis of the dielectric resonator as in Figure 12, of diameter 0.5" and height 0.2", made of a dielectric of relative permittivity 24. In Figure 13, each minimum of the  $|S_{11}|$  indicates a resonant mode. About 35 modes are detected in the frequency range of 5–17 GHz. Further 3-D FDTD analysis of the problem becomes challenging for several reasons:

- fine meshing is needed for accurate determination of the resonant modes, which makes the 3-D analysis quite time consuming
- the resonant frequencies are so numerous that it is difficult to apply special signal-processing methods (like Prony method) to detect them
- it is very difficult to obtain a clear picture of the field distribution of different modes of very close resonant frequencies.

All the above problems are effectively resolved when we apply the V2-D simulation running it separately for different values of  $n$ . In the considered example and in the band of 5–17 GHz, we detect one mode for  $n = 7$ , two modes for  $n = 6$ , four modes for  $n = 5$ , five modes for  $n = 4$ , six modes for  $n = 3$ , nine modes for  $n = 2$ , eleven modes for  $n = 1$ , and five modes for  $n = 0$ . This makes a total of 43 modes, significantly more than for a less accurate 3-D simulation results of Figure 13. There is also no problem in obtaining field patterns even for closely positioned resonances. For example, Figures 14 and 15 present distributions of the angular E-field component for the modes at 16.355 GHz, and 16.390 GHz, respectively. The mode at 16.355 GHz is a whispering gallery mode

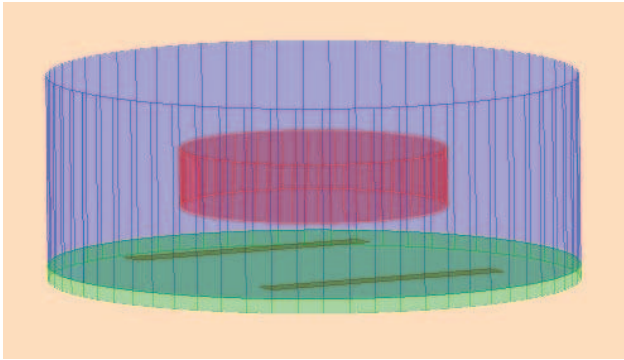


**Figure 12.** A dielectric resonator (red pill) coupled to two microstrip lines (dark green).

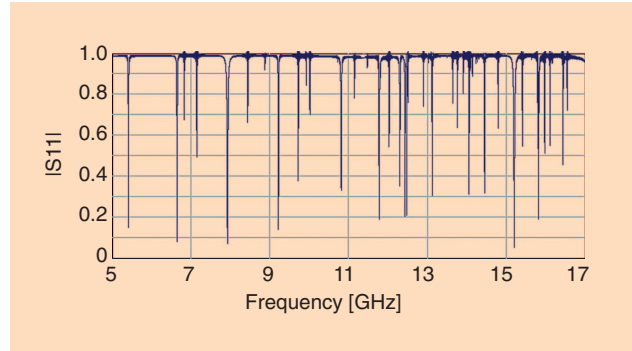


**Figure 13.** Reflection characteristics of the resonator of Figure 12 obtained by 3-D FDTD. Minima indicate the detected resonant modes.

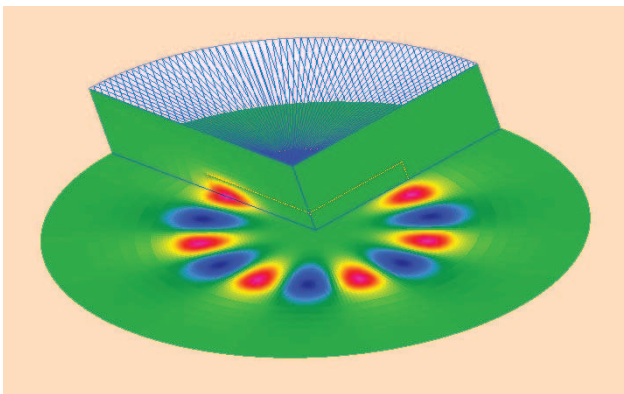


**Figure 14.** A whispering gallery mode in the resonator of Figure 12 at  $f = 16.355$  GHz.

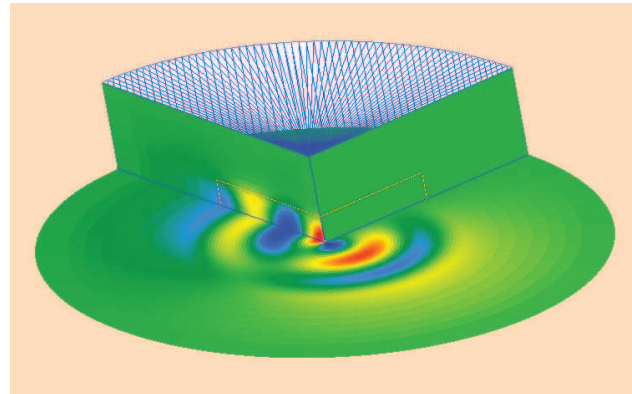


**Figure 15.** A mode with unity angular dependence in the resonator of Figure 12 at  $f = 16.390$  GHz.

with  $n = 7$  and field concentration along the edge of the dielectric. Its unloaded Q-factor is determined by the properties of the dielectric and may be even close to 100,000. The mode of Figure 15 has  $n = 1$  and different Q-factor properties. Fields are spread over the surrounding space and will surely reach the walls of the metal box. Thus the possibilities of obtaining a high Q are very limited.

### How to Do More and Better

General purpose EM software packages have become practical tools in the design of many microwave and millimeter wave components, antennas, and systems. Yet in many other cases, the engineers' (and managers') desire to do more and better can only be satisfied with customized methods.

In this article, we have focused on the V2-D FDTD method for axisymmetrical devices, also known as BOR FDTD. The concept of BOR FDTD is not new. Our specific formulation dates back to 1988 [21], and publications on the subject by various groups were particularly abundant throughout the 1990s [19]–[27]. However, what may be striking to the reader, is that the same software tool can be used in such allegedly diverse fields as coaxial connectors design and Gaussian beam forming for optical frequency range, in searching for radiation patterns of large reflector antennas, as well as in Q-factor calculations of dielectric resonators.

The approach to solving Maxwell equations by the V2-D FDTD method is straightforward and easily understood by an engineer. Not only the whole structure simulation is feasible, facilitating a search for globally optimum solutions, but also a valuable insight is provided into the subtleties of the device operation in the 3-D space and time. A graphical interface of the QW-V2D solver has been used here to exemplify how the software helps in problem solving and quick search for new solutions.

### References

- [1] Taflove and S.C. Hagness, *Computational Electromagnetics—The Finite-Difference Time-Domain Method*, 3rd ed. Norwood, MA: Artech House, 2005.
- [2] QuickWave-3D and QW-V2D, QWED Sp. z o.o., 1997–2008. [Online]. Available: <http://www.qwed.com.pl>
- [3] Concerto, Vector Fields—ERA Technology Ltd., 1999–2008. [Online]. Available: <http://www.vectorfields.com>
- [4] CST Microwave Studio, CST GmbH, 1998–2008, [Online]. Available: <http://www.cst.com>
- [5] O.C. Zienkiewicz, R.L. Taylor, and J.Z. Zhu, *Finite Element Method—Its Basis & Fundamentals*, 6th ed. London, U.K.: Elsevier Butterworth-Heinemann, 2005.
- [6] HFSS, Ansoft, Inc., 1990–2008, [Online]. Available: <http://www.ansoft.com>
- [7] Sonnet Suites, Sonnet Software, Inc., 1983–2008, [Online]. Available: <http://www.sonnetsoftware.com>
- [8] IE3D, Zeland Software, Inc., 1997–2008, [Online]. Available: <http://www.zeland.com>

- [9] C. Mroczkowski and W.K. Gwarek, "Microwave circuits described by two-dimensional vector wave equation and their analysis by FD-TD method," in *Proc. 21st European Microwave Conf.*, Stuttgart, Sept. 1991, pp. 199–204.
- [10] W.K. Gwarek, T. Morawski, and C. Mroczkowski, "Application of the FD-TD method to the analysis of circuits described by the two-dimensional vector wave equation," *IEEE Trans. Microwave Theory Tech.*, vol. MTT-41, no. 2, pp. 311–317, Feb. 1993.
- [11] G. Zheng and K. Chen, "Effects of substrate anisotropy on the dispersion of transient signals in microstrip lines," *Int. J. Infrared Millimeter Waves*, vol. 11, no. 4, pp. 489–498, 1990.
- [12] H. Jin, R. Vahldieck, and S. Xiao, "A full-wave analysis of arbitrary guiding structures using a two-dimensional TLM mesh," in *Proc. 21st European Microwave Conf.*, Stuttgart, Sept. 1991, pp. 205–210.
- [13] H. Jin, R. Vahldieck, and S. Xiao, "Full-wave analysis of guiding structures using a 2-D array of 3-D TLM nodes," *IEEE Trans. Microwave Theory Tech.*, vol. MTT-41, no. 3, pp. 472–477, Mar. 1993.
- [14] S. Xiao, R. Vahldieck, and H. Jin, "Full-wave analysis of guided wave structures using a novel 2-D FD-TD," *IEEE Microwave and Guided Wave Lett.*, vol. 2, no. 5, pp. 165–167, May 1992.
- [15] A. Asi and L. Shafai, "Dispersion analysis of anisotropic inhomogeneous waveguides using compact 2D-FDTD," *Electronics Lett.*, vol. 28, no. 15, pp. 1451–1452, July 1992.
- [16] M. Celuch-Marcysiak and W.K. Gwarek, "Time-domain analysis of dispersive transmission lines," *J. Physique III*, vol. 3, pp. 581–591, Mar. 1993.
- [17] M. Celuch-Marcysiak and W.K. Gwarek, "A transformed symmetrical condensed node for the effective TLM analysis of guided wave problems," *IEEE Trans. Microwave Theory Tech.*, vol. MTT-41, no. 5, pp. 820–823, May 1993.
- [18] M. Celuch-Marcysiak and W.K. Gwarek, "Spatially looped algorithms for time-domain analysis of periodic structures," *IEEE Trans. Microwave Theory Tech.*, vol. MTT-43, no. 4, pp. 860–865, Apr. 1995.
- [19] G. Aharonian, R. Meller, and R.H. Siemann, "Transverse wakefield calculations," *Nucl. Instrum. Methods*, vol. 212, no. 1-3, pp. 23–35, July 1983.
- [20] T.G. Jurgens, G.W. Saewert, and F.A. Harfoush, "XWAKE 1.0: A new tool for wakefield and impedance calculations," in *Proc. 4th European Particle Accelerator Conf.*, London, June 1994, pp. 1318–1320.
- [21] W.K. Gwarek, "Computer-aided analysis of arbitrarily-shaped coaxial discontinuities," *IEEE Trans. Microwave Theory Tech.*, vol. MTT-36, no. 2, pp. 337–342, Feb. 1988.
- [22] D.B. Davidson and R.W. Ziolkowski, "Body of revolution FDTD modeling of space time focusing by a three dimensional lens," *J. Opt. Soc. America A*, vol. 11, no. 4, pp. 1471–1490, Apr. 1994.
- [23] J.C. Maloney, G.S. Smith, and W.R. Scott, "Accurate computation of the radiation from simple antennas using the finite-difference time-domain method," *IEEE Trans. Antennas Propag.*, vol. 38, no. 7, pp. 1059–1068, July 1990.
- [24] M. Rammal, P. Roy, Ph. Dufrane, and B. Jecko, "Rigorous design of omnidirectional antennas using the FDTD method," *Microwave Eng. Europe*, pp. 37–41, June/July 1997.
- [25] Y. Chen, R. Mittra, and P. Harms, "Finite-difference time-domain algorithm for solving Maxwell's equations in rotationally symmetric geometries," *IEEE Trans. Microwave Theory Tech.*, vol. MTT-44, no. 6, pp. 832–839, June 1996.
- [26] C. Mroczkowski, M. Celuch-Marcysiak, and W.K. Gwarek, "Joint application of superabsorption and near-to-far field transform to FDTD analysis of axisymmetrical antennas," in *Proc. 24th European Microwave Conf.*, Cannes, Sept. 1994, pp. 899–904.
- [27] M. Celuch-Marcysiak and W.K. Gwarek, "Improved and simpler FDTD formulation for axisymmetrical problems," in *Proc. 2000 IEEE-AP-S Int. Symp.*, Salt Lake City, July 2000, vol. 1, pp. 228–231.
- [28] P. Kozakowski and M. Mrozowski, "Low-order models form FD-TD time samples," *IEEE Microwave Wireless Components Lett.*, vol. 12, no. 11, pp. 438–440, Nov. 2002.
- [29] M. Le Goff, "Etude et développement d'un banc de mesure quasi-optique pour la caractérisation de composants passifs et actifs: application à la définition d'une structure d'amplificateur quasi-optique," Ph.D. dissertation, Université de Bretagne Occidentale, France, 1999. 